



X-ray production cross sections for Ir and Bi M-subshells induced by electron impact

M.D. Décima, G.E. Castellano, J.C. Trincavelli, A.C. Carreras*

Instituto de Física Enrique Gaviola (IFEG-CONICET), Facultad de Matemática, Astronomía, Física y Computación (FAMAF), Universidad Nacional de Córdoba, Córdoba, Argentina

ARTICLE INFO

Keywords:

X-ray production cross section
Ionization cross section
X-ray emission
M subshells
Iridium
Bismuth

ABSTRACT

M-subshell X-ray production cross sections were indirectly measured for Ir and Bi targets irradiated with monoenergetic electron beams. The projectile energy range ran from 2.2 to 28 keV, impinging on Ir and Bi pure bulk targets in a scanning electron microscope. The resulting X-ray emission spectra were acquired with an energy dispersive spectrometer, and processed afterwards by means of a robust parameter optimization procedure developed previously. X-ray production cross sections were finally obtained through an approach involving an analytical prediction for the emission spectra, which relies on the ionization depth distribution function. The values obtained by this approach were compared with empirical and theoretical predictions, appealing to different relaxation data taken from the literature.

1. Introduction

The ionization cross section σ is a magnitude proportional to the probability of ionizing an atom, which is experimentally unavailable if certain relaxation parameters are unknown. The experimental determination of these relaxation parameters is, in turn, rather complicated. On the other hand, σ can be assessed on the basis of different theoretical models, and experimental validation of these predictions is convenient.

The X-ray production cross section σ^x , instead, can be experimentally obtained, and it allows for the determination of σ , provided the relaxation parameters mentioned are known. Thus, a comparison between the theoretical σ and the experimental σ^x can be performed when a reliable set of relaxation parameters is accessible.

The availability of experimental results for σ^x decreases for less bound atomic levels. In this sense, experimental absolute determinations for separate M sublevels are reduced to a few elements. Particularly, results corresponding to overvoltages compatible with the most usual X-ray spectroscopic techniques were obtained for Au, Bi [1], Pb [2], Th [3] and U [4], using thin targets, and more recently, Pt, Au [5], Re and Os [6] by means of a bulk-target method based on ionization depth distribution functions.

In this work, spectra induced by electron incidence on thick targets were used to determine the X-ray production cross section curves corresponding to the M_5 , M_4 and M_3 levels of iridium and bismuth. In addition, data were also jointly obtained for the M_1+M_2 subshells.

2. Experimental

The Ir and Bi spectra used for the determination of σ^x were produced by electron incidence in a Carl Zeiss Sigma field emission scanning microscope, and recorded with an energy dispersive spectrometer (EDS) based on an Oxford silicon drift detector, whose front window is an ultrathin polymer layer, supported by a silicon grid 380 μm thick with 77% open area. The detector energy resolution is 150 eV, defined as the full width at the half maximum of the $\text{Cu-K}\alpha$ line (8.04 keV).

The efficiency of an X-ray detector for a given photon energy is the product of the intrinsic efficiency—*i.e.*, the fraction of photons arriving at the detector that are indeed registered—and the solid angle fraction subtended by the detector from the beam impact point on the sample surface. Both issues were described in a previous work [5], and the same detector and experimental geometry were used here.

The samples were pure bulk standards mounted on a non-conductive resin within a brass block (Micro-Analysis Consultants Ltd), which is coated with a carbon thin layer to furnish thermal and electric conductivity. The cross section curves were surveyed using an electron beam impinging perpendicularly to the sample surface with energies ranging from 2.2 to 28 keV. The spectra were collected at a 35° take-off angle during acquisition live times between 120 and 360 s, with beam currents from 140 to 1300 pA, measured with a Faraday cup before and after recording each spectrum. For illustration purposes, Ir and Bi spectra induced by a 20 keV electron beam are shown in Fig. 1.

* Corresponding author.

E-mail address: alejocarreras@unc.edu.ar (A.C. Carreras).

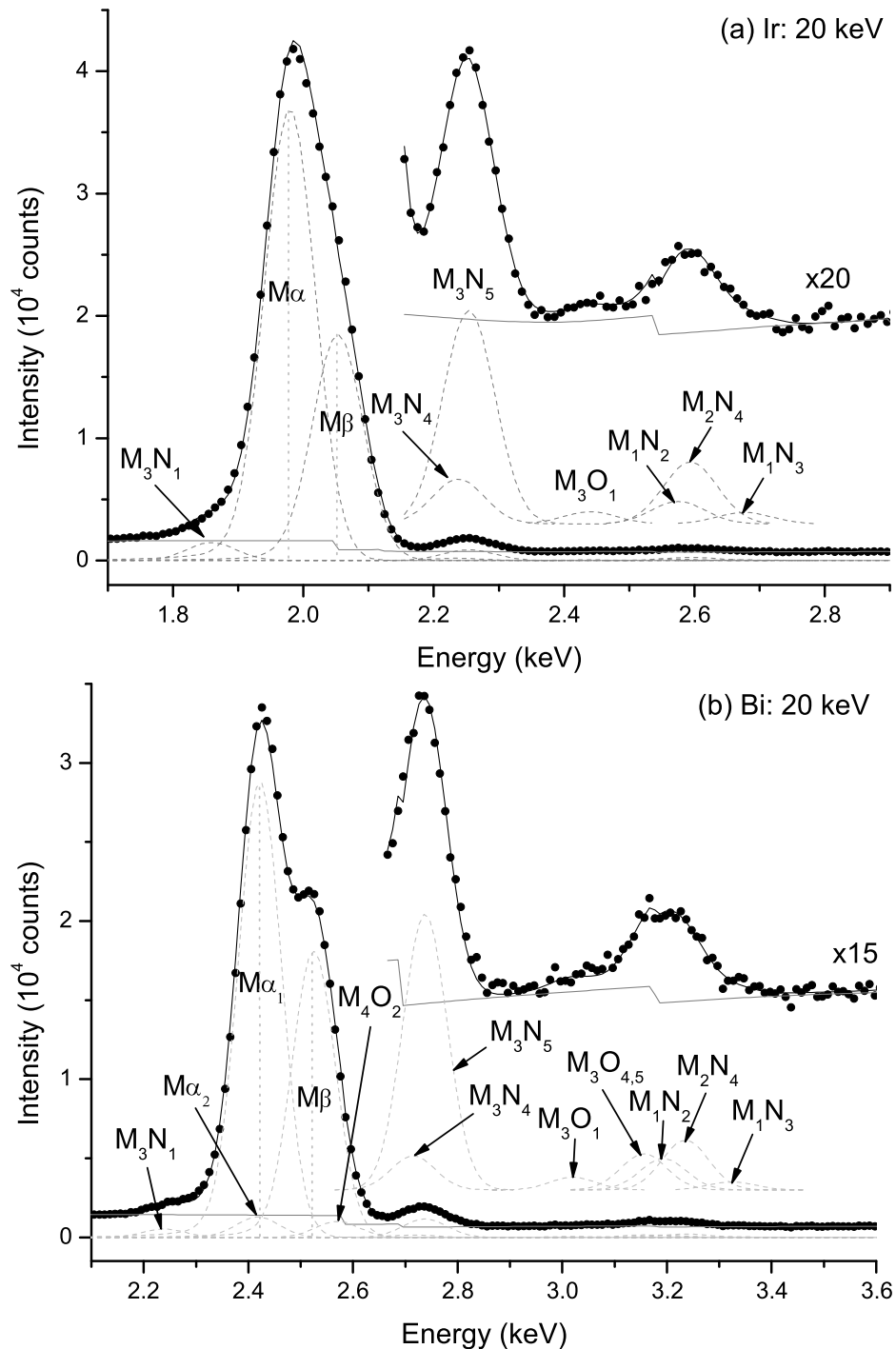


Fig. 1. EDS X-ray spectra for iridium (a) and bismuth (b) including decays to M vacancies induced by a 20 keV electron beam. Insets display magnified views for weak emissions. Dots: experimental data; solid black line: fit; dotted lines: individual contribution of each transition; solid gray line: background.

3. Methodology

Values for σ^x were obtained from the measured data through a spectral processing carried out by means of the software POEMA [7]. The method implemented in this package consists in minimizing the quadratic differences between the experimental spectrum and an analytical function proposed to describe it, which depends on certain physical and instrumental parameters. These parameters can be obtained as a result of the optimization procedure, the whole spectral processing method being detailed in a recent contribution [5].

The characteristic peaks were described by Gaussian profiles with an asymmetric correction to account for the low energy tail due to incomplete charge collection in the EDS X-ray detector [8]. Regarding the spectrum background, it was modeled by means of an analytical function for the bremsstrahlung, which was previously developed [9]. A polynomial correction in the low energy region was implemented for a better description of the weakest lines.

As mentioned in Section 2, a carbon layer coats the standard block to make it conductive, which imposes as side effects the degradation of the monoenergetic incident electron beam and the attenuation of the emerging X-rays in their way to the detector. To account for the

Table 1

X-ray production cross sections for iridium. Numbers in parentheses indicate the estimated uncertainties in the last digits, which correspond to one standard deviation. The uncertainties associated with incident energies are below 0.5%.

E_o (keV)	σ_{1+2}^x (barn)	σ_3^x (barn)	σ_4^x (barn)	σ_5^x (barn)
2.215	–	–	110(20)	220(40)
2.761	–	8(9)	200(50)	430(90)
3.297	2(1)	20(10)	290(60)	600(120)
3.826	6(1)	33(6)	350(30)	700(60)
4.853	11(2)	48(6)	420(30)	800(50)
5.882	13(2)	50(6)	420(30)	830(50)
6.934	14(2)	50(5)	420(30)	810(40)
7.976	15(1)	51(5)	410(30)	780(40)
8.905	15(2)	54(5)	400(30)	760(40)
9.984	13(1)	53(5)	380(30)	720(40)
11.983	12(2)	49(6)	310(20)	610(30)
15.004	11(2)	40(7)	240(20)	490(30)
20.139	10(2)	38(8)	220(30)	430(30)
28.080	9(6)	30(20)	170(50)	370(60)

influence of this effect, the conductive layer thickness was determined from the carbon $K\alpha$ peak intensity, as detailed in a previous work [5]. The thickness obtained was $z_c = (22.1 \pm 0.8)$ nm.

The energy E_o of the electrons reaching the standard surface can thus be written as

$$E_o = E_{DH} - (S/\rho)\rho z_c, \quad (1)$$

where E_{DH} is the Duane–Hunt energy [10], S/ρ is the mass stopping power of carbon at E_{DH} , and ρz_c is the carbon layer mass thickness. E_{DH} was assessed from a linear fit performed to the high energy region of the spectrum, and the stopping power was taken from the databases included in the PENELOPE package [11].

In the case of iridium, a strong overlapping between the M_3N_1 line and the asymmetric tail of the $M\alpha$ peak ($M_5N_{6,7}$ transition) was found. This overlapping hampered the refinement of the peak asymmetry due to incomplete charge collection in the detector. To overcome this problem, the strategy used consisted in avoiding these problematic channels, since the remaining numbers of counts were high enough to provide a reliable fit (see Fig. 1a). Instead, it was possible to account for the mentioned asymmetric behavior in the spectral fitting of bismuth, since overlapping effects were quite lower (see Fig. 1b).

Regarding characteristic energies, all the values for bismuth were taken from a previous work [12], except for M_5N_7 , which corresponds to Bearden database [13]. For iridium, the data were taken from Ref. [13], except for the M_3O_1 and M_1N_2 transitions, absent in Bearden's publication, for which the values reported by Perkins et al. [14] were considered. All the characteristic energies were kept fixed during the optimization procedure.

The X-ray production cross sections σ_k^x were obtained from the optimization of the peak scale factors C_k corresponding to the M_k subshells:

$$C_k = N_e \sigma_k^x \frac{\Delta\Omega}{4\pi}, \quad (2)$$

where N_e is the number of incident electrons and $\Delta\Omega$ is the solid angle subtended by the detector.

4. Results and discussion

The values obtained for the X-ray production cross sections corresponding to the M subshells of Ir and Bi are gathered in Tables 1 and 2, and plotted in Figs. 2 and 3, respectively. The results corresponding to M_1 and M_2 subshells were obtained from weak and strongly overlapped diagram lines, as can be seen in Fig. 1; for this reason they could not be derived separately. Instead, the combined contribution of both subshells is reported.

Table 2

X-ray production cross sections for bismuth. Numbers in parentheses indicate the estimated uncertainties in the last digits, which correspond to one standard deviation. The uncertainties associated with incident energies are below 0.5%.

E_o (keV)	σ_{1+2}^x (barn)	σ_3^x (barn)	σ_4^x (barn)	σ_5^x (barn)
2.758	–	–	–	180(20)
3.269	–	–	182(8)	330(20)
3.811	–	16.8(8)	260(10)	450(20)
4.325	–	34(2)	320(10)	550(20)
4.881	11.4(7)	38(2)	360(20)	600(30)
5.875	13.4(8)	46(3)	400(20)	660(30)
6.911	14.5(7)	55(3)	430(20)	680(30)
7.902	15.8(8)	59(3)	430(20)	680(30)
8.946	15.5(9)	60(4)	420(20)	680(30)
9.916	15(1)	62(4)	410(20)	650(30)
12.013	14(1)	59(5)	360(20)	570(30)
15.059	11(1)	50(5)	290(20)	450(30)
20.128	11(1)	49(6)	270(20)	410(20)
27.884	9(2)	40(10)	220(20)	360(20)

To provide an estimate for the uncertainty in σ^x , the errors associated with the number of incident electrons N_e , with the detector solid angle $\Delta\Omega$, and with the peak scale factor C_k obtained from the spectral fitting, were propagated in Eq. (2). To obtain the uncertainty of the latter, a procedure described previously [15] was followed, which consists in propagating the errors in the number of counts registered at each energy channel, through numerical differentiation.

On the other hand, the error in E_o , always below 0.5%, was estimated by propagating the uncertainties of E_{DH} and z_c in Eq. (1), and neglecting the errors in the stopping power. The uncertainty associated with E_{DH} was assessed from the uncertainties associated with the linear fit performed to obtain E_{DH} .

The X-ray production cross section corresponding to the M_k subshell, σ_k^x , can be written as

$$\sigma_k^x = \omega_k \bar{\sigma}_k,$$

where ω_k is the fluorescence yield and $\bar{\sigma}_k$ is the final vacancy production cross section, which in turn, is related to the ionization cross sections σ_k as follows:

$$\bar{\sigma}_1 = \sigma_1$$

$$\bar{\sigma}_2 = \sigma_2 + f_{12}\bar{\sigma}_1$$

$$\bar{\sigma}_3 = \sigma_3 + f_{13}\bar{\sigma}_1 + f_{23}\bar{\sigma}_2$$

$$\bar{\sigma}_4 = \sigma_4 + f_{14}\bar{\sigma}_1 + f_{24}\bar{\sigma}_2 + f_{34}\bar{\sigma}_3$$

$$\bar{\sigma}_5 = \sigma_5 + f_{15}\bar{\sigma}_1 + f_{25}\bar{\sigma}_2 + f_{35}\bar{\sigma}_3 + f_{45}\bar{\sigma}_4,$$

f_{ij} being the probability for a Coster–Kronig transition from M_j to M_i subshells, which includes the partial widths of both radiative and non-radiative contributions. For incidence energies greater than the L ionization edges, vacancies in this shell must be considered, and the terms

$$\sigma_{L_1} n_{L_1 M_k} + \sigma_{L_2} n_{L_2 M_k} + \sigma_{L_3} n_{L_3 M_k}$$

must be added to $\bar{\sigma}_k$, where $n_{L_i M_k}$ stands for the transition probability from M_k to L_i subshells. For the beam energy range involved here, K vacancies are not created.

In Figs. 2 and 3, a comparison with theoretical [16] and empirical [17] data derived from the ionization cross sections σ_k is presented. With the purpose of comparing the σ_k^x values obtained here with other sources of data, it was necessary to rely on the combination of analytical curves of ionization cross section along with relaxation parameters published by other authors. For the present comparisons, the σ values used were those reported by Bote and Salvat [16], based on the distorted wave Born approximation (DWBA), as well as empirical data published by Casnati et al. [17], as can be seen in Figs. 2 and 3. Regarding the relaxation parameters, several sources of ω_k [14,18]

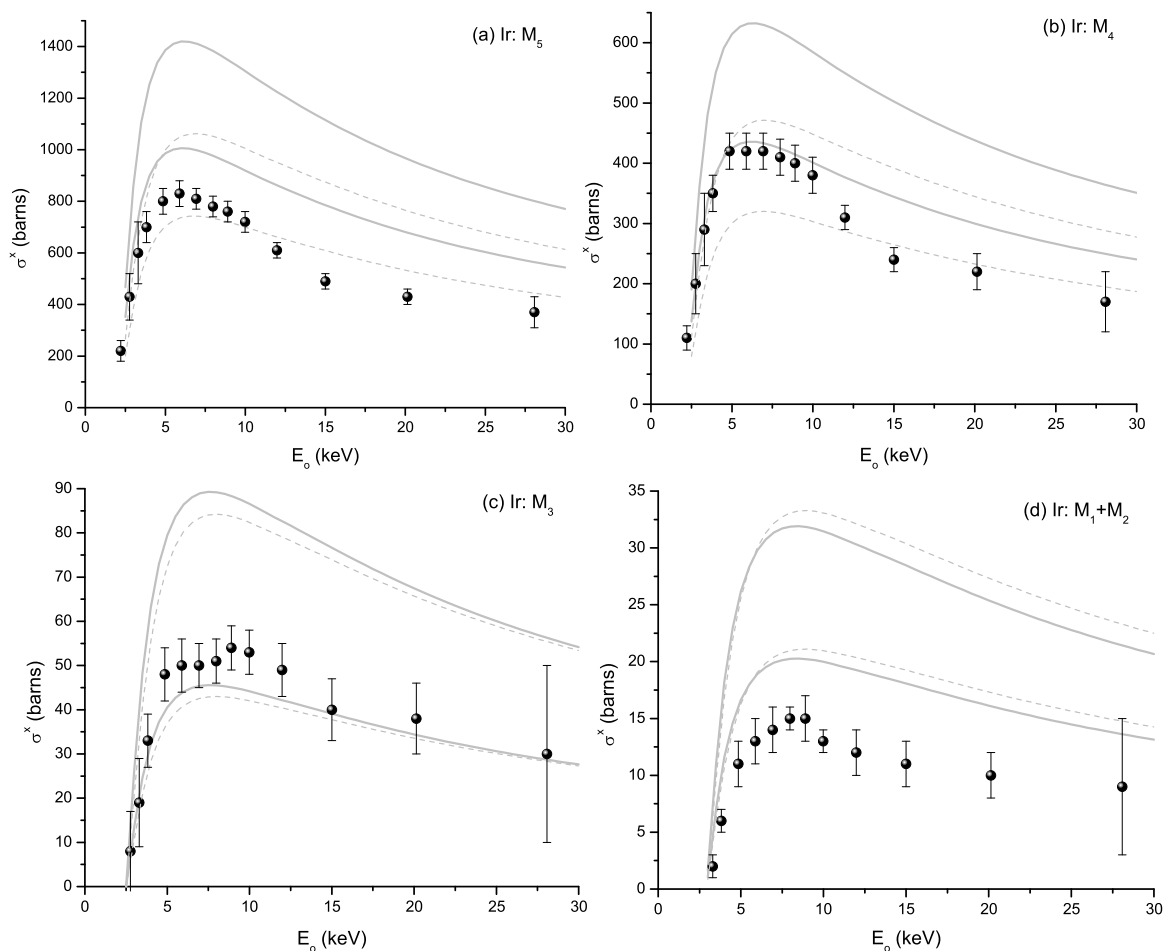


Fig. 2. X-ray production cross sections for iridium. Solid spheres: this work. Gray lines delimitate intervals for the σ^x resulting values when combining theoretical or empirical data for ionization cross sections with different combinations of relaxation parameters; solid line: Bote and Salvat [16], dashed line: Casnati et al. [17]. (a) M_5 subshell; (b) M_4 subshell; (c) M_3 subshell; (d) M_1+M_2 subshells.

Table 3
Coster-Kronig coefficients and fluorescence yields used for comparison.

Ref.	ω_{M_1}	ω_{M_2}	ω_{M_3}	ω_{M_4}	ω_{M_5}	f_{45}	f_{12}	f_{13}	f_{14}	f_{15}	f_{23}	f_{24}	f_{25}	f_{34}	f_{35}
Ir [14]	0.00303	0.00548	0.00694	0.0254	0.0262	0.091	0.128	0.594	0.077	0.108	0.089	0.578	0.092	0.067	0.615
Ir [22]	0.00186	0.00357	0.00355	0.0183	0.0230										
Ir [18]						0.419	0.148	0.564	0.072	0.121	0.115	0.701	0.069	0.110	0.781
Bi [14]	0.00417	0.00689	0.00920	0.0377	0.0373	0.059	0.117	0.598	0.081	0.112	0.087	0.581	0.091	0.079	0.543
Bi [22]	0.00291	0.00666	0.00532	0.0329	0.0322										
Bi [18]						0.055	0.099	0.604	0.072	0.123	0.118	0.686	0.059	0.083	0.774

and f_{ij} [14,18–23] were considered. Each of the models for σ used in the comparison was combined with the different relaxation parameters mentioned (Table 3), the upper and lower bounds for these possible choices being displayed in these Figures. The upper bounds correspond to the values for ω_k reported by Perkins et al. [14] with the f_{ij} data published by Söğüt et al. [18], while the lower bounds was obtained using the f_{ij} probabilities given by Perkins et al. [14] combined with the ω_k values fitted by Kaur and Mittal [22] to McGuire's data [23].

In addition, experimental data for the bismuth M_5 subshell given by Merlet et al. [1] were compared with the present results (see Fig. 3a), whereas experimental values for the other cases are not available in the literature, to the best of the authors' knowledge.

A noticeable discrepancy can be observed in Figs. 2 and 3 between the values resulting from the two sets of ionization cross section data used, for the M_5 and M_4 subshells, whereas for M_3 and M_1+M_2 the predictions are similar. On the other hand, the experimental results obtained here are in reasonable agreement with the analytical results

available, except for M_1+M_2 , for which the predictions are above the values obtained in the present work.

In the only case for which the present data were compared to experimental results, the former are below the latter. The values obtained by Merlet et al. [1] agree with DWBA calculations, whereas the present results are in good agreement with the empirical model proposed by Casnati et al. [17]

For the elements studied here, the $M\beta$ line (M_4N_6 transition) is close to the M_5 absorption edge. For this reason, the estimation for the $M\beta$ emission generated intensity is very sensitive to the edge energy E_{M_5} : if $E_{M\beta} > E_{M_5}$, there is a strong self absorption, whereas if $E_{M\beta} < E_{M_5}$, the $M\beta$ line absorption is similar to that of the $M\alpha$ line, because none of them can excite the M_5 level.

Following the criterion established in a previous study [24], the value chosen along this work for the iridium E_{M_5} edge energy was 2061 eV, above the $E_{M\beta}$ energy. It must be noted that this value is different from the most used data available in the literature (2040.4 eV, according to [25,26]), for which $E_{M\beta} > E_{M_5}$. The values that would

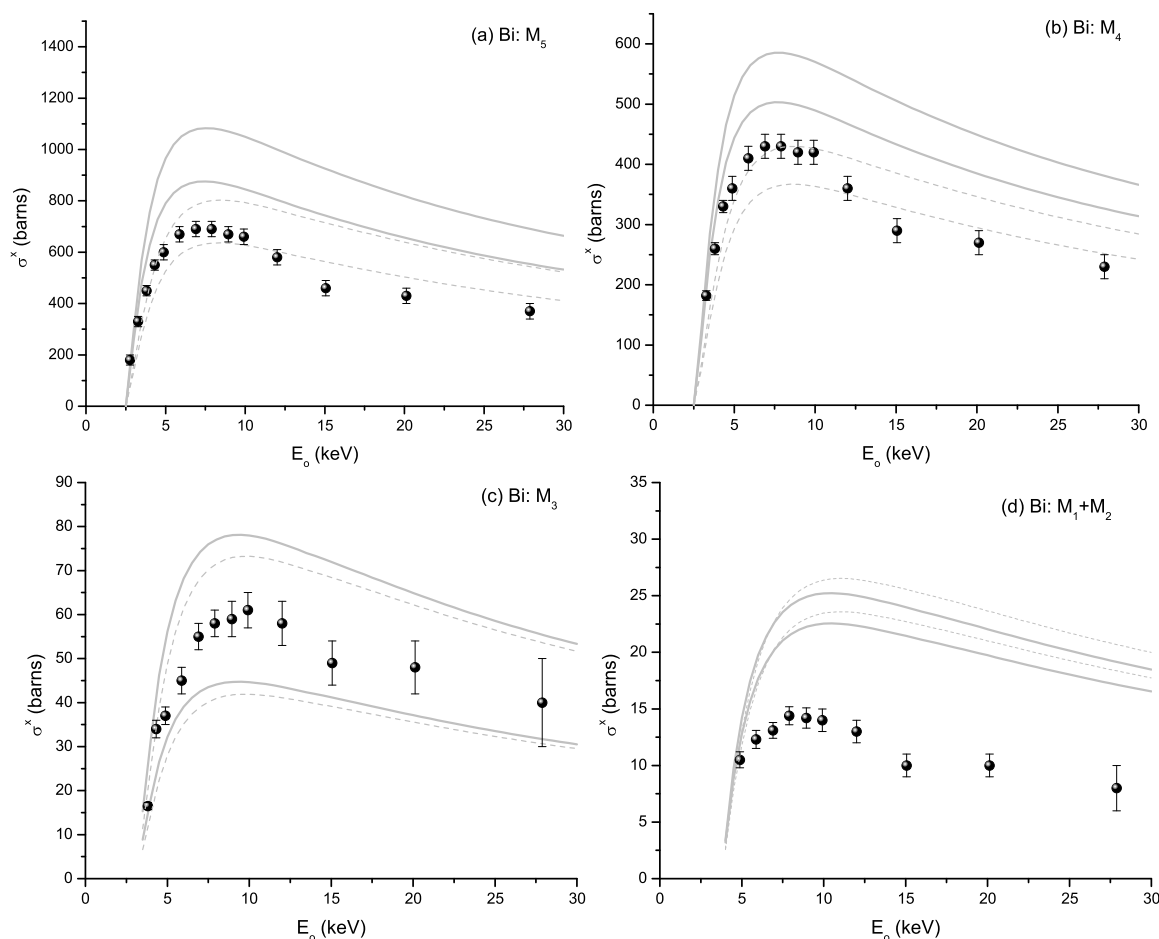


Fig. 3. X-ray production cross sections for bismuth. Solid spheres: this work. Empty circles: experimental data from Merlet et al. [1]. Gray lines delimitate intervals for the σ^x resulting values when combining theoretical or empirical data for ionization cross sections with different combinations of relaxation parameters; solid line: Bote and Salvat [16], dashed line: Casnati et al. [17]. (a) M_5 subshell; (b) M_4 subshell; (c) M_3 subshell; (d) M_1+M_2 subshells.

be obtained for σ_4^x of iridium taking E_{M5} from these references, would exhibit an anomalous behavior, lying above the corresponding σ_5^x at high energies, due to an overestimation of $M\beta$ -line absorption. Instead, the E_{M5} values tabulated for bismuth are clearly above $E_{M\beta}$, which does not introduce any complication in estimating the $M\beta$ absorption.

5. Conclusion

Experimental data for the X-ray production cross sections under electron irradiation on thick targets have been obtained for Ir- and Bi-M subshells, by means of a method developed previously on the basis of the ionization depth distribution function. The results obtained were compared to theoretical and empirical data, whereas a comparison to experimental data available in the literature only was possible for the case of the bismuth M_5 subshell.

The absorption edge location is very important in the determination of cross sections using thick targets in cases such as iridium, for which the $M\beta$ line is very close to the M_5 edge. For this reason, the experimental determination of M-edge positions is of interest for elements in certain atomic number range. Nevertheless, the characterization of absorption edges is usually difficult, since they are often too close to some diagram line, which masks the edge position, even using a wavelength dispersive spectrometer.

CRedit authorship contribution statement

M.D. Décima: Formal analysis, Investigation, Methodology. **G.E. Castellano:** Formal analysis, Investigation, Methodology, Software,

Writing – original draft, Writing – review & editing. **J.C. Trincavelli:** Conceptualization, Data curation, Formal analysis, Investigation, Methodology, Software, Writing – original draft, Writing – review & editing. **A.C. Carreras:** Conceptualization, Data curation, Formal analysis, Funding acquisition, Investigation, Methodology, Supervision, Writing – original draft, Writing – review & editing.

Declaration of competing interest

The authors declare that they have no known competing financial interests or personal relationships that could have appeared to influence the work reported in this paper.

Data availability

Data will be made available on request.

Acknowledgments

This work was financially supported by the Secretaría de Ciencia y Técnica of the Universidad Nacional de Córdoba (UNC), Argentina. The authors are also grateful to the Laboratorio de Microscopía y Análisis por Rayos X (LAMARX-UNC), where the experimental determinations were performed.

References

- [1] C. Merlet, X. Llovet, F. Salvat, Near-threshold absolute M-shell X-ray production cross sections of Au and Bi by electron impact, *Phys. Rev. A* 78 (2008) 022704.
- [2] A. Moy, C. Merlet, X. Llovet, O. Dugne, Measurements of absolute L- and M-subshell X-ray production cross sections of Pb by electron impact, *J. Phys. B: At. Mol. Opt. Phys.* 46 (11) (2013) 115202.
- [3] A. Moy, C. Merlet, O. Dugne, Measurements of absolute M-subshell X-ray production cross sections of Th by electron impact, *Chem. Phys.* 440 (2014) 18–24.
- [4] A. Moy, C. Merlet, X. Llovet, O. Dugne, M-subshell ionization cross sections of U by electron impact, *J. Phys. B: At. Mol. Opt. Phys.* 47 (5) (2014) 055202.
- [5] A. Carreras, G. Castellano, S. Segui, J. Trincavelli, Experimental X-ray-production cross sections for the M_3 , M_4 , and M_5 subshells of Pt and Au by electron impact, *Phys. Rev. A* 102 (2020) 012817.
- [6] A. Aguilar, G. Castellano, S. Segui, J. Trincavelli, A. Carreras, M-subshell X-ray production cross sections of Re and Os by electron impact, *J. Anal. At. Spectrom.* 111 (2023) 111–112.
- [7] R. Bonetto, G. Castellano, J. Trincavelli, Optimization of parameters in electron probe microanalysis, *X-Ray Spectrom.* 30 (2001) 313–319.
- [8] C. Visňovezky, S. Limandri, M.E. Canafoglia, R. Bonetto, J. Trincavelli, Asymmetry of characteristic X-ray peaks obtained by a Si(Li) detector, *Spectrochim. Acta Part B*. 62 (2007) 492–498.
- [9] G. Castellano, J. Osán, J. Trincavelli, Analytical model for the bremsstrahlung spectrum in the 0.25–20 keV photon energy range, *Spectrochim. Acta B: Atom. Spectrosc.* 59 (3) (2004) 313–319.
- [10] W. Duane, F. Hunt, On X-Ray wave-lengths, *Phys. Rev.* 6 (1915) 166–172.
- [11] F. Salvat, J. Fernández-Varea, J. Sempau, PENELOPE 2011: A Code System for Monte Carlo Simulation of Electron and Photon Transport, OECD Nuclear Energy Agency, Issy les Moulineaux, France, 2011.
- [12] S. Limandri, J. Trincavelli, R. Bonetto, A. Carreras, Structure of the Pb, Bi, Th and U M X-ray spectra, *Phys. Rev. A* 78 (2008) 022518 1–10, <http://dx.doi.org/10.1103/PhysRevA.78.022518>.
- [13] J.A. Bearden, X-ray wavelengths, *Rev. Modern Phys.* 39 (1967) 78, <http://dx.doi.org/10.1103/RevModPhys.39.78>.
- [14] S.T. Perkins, D.E. Cullen, M.H. Chen, J.H. Hubbell, J. Rathkopf, J.H. Scofield, Tables and Graphs of Atomic Subshell and Relaxation Data Derived from the LLNL Evaluated Atomic Data Library (EADL), $Z=1-100$, Lawrence Livermore National Laboratory Report UCRL-50400 30, 1991, p. 1.
- [15] R.D. Bonetto, A.C. Carreras, J.C. Trincavelli, G.E. Castellano, L-shell radiative transition rates by selective synchrotron ionization, *J. Phys. B* 37 (2004) 1477, <http://dx.doi.org/10.1088/0953-4075/37/7/009>.
- [16] D. Bote, F. Salvat, Calculations of inner-shell ionization by electron impact with the distorted-wave and plane-wave Born approximations, *Phys. Rev. A* 77 (2008) 042701, <http://dx.doi.org/10.1103/PhysRevA.77.042701>.
- [17] E. Casnati, A. Tartari, C. Baraldi, An empirical approach to K-shell ionisation cross section by electrons, *J. Phys. B At. Mol. Phys.* 15 (1982) 155–167.
- [18] Ö. Söğüt, E. Büyükkasap, A. Küçükönder, M. Ertuğrul, O. Doğan, H. Erdoğan, Ö. Şimşek, Fit values of M subshell fluorescence yields and Coster-Kronig transitions for elements with $20 \leq Z \leq 90$, *X-Ray Spectrom.* 31 (1) (2002) 62–70, <http://dx.doi.org/10.1002/xrs.539>.
- [19] Y. Chauhan, S. Puri, M_i ($i=1-5$) subshell fluorescence and Coster-Kronig yields for elements with $67 \leq Z \leq 92$, *At. Data Nucl. Data Tables* 94 (1) (2008) 38–49.
- [20] M.H. Chen, B. Crasemann, H. Mark, Relativistic M-shell radiationless transitions, *Phys. Rev. A* 21 (2) (1980) 449–453.
- [21] M.H. Chen, B. Crasemann, H. Mark, Radiationless transitions to atomic $M_{1,2,3}$ shells: Results of relativistic theory, *Phys. Rev. A* 27 (6) (1983) 2989–2994.
- [22] G. Kaur, R. Mittal, M sub-shell fluorescence and Coster-Kronig yield data generation for elements, $57 \leq Z \leq 90$ (computer code 'MFCKYLD'), *J. Quant. Spectrosc. Radiat. Transfer* 133 (2014) 489–503.
- [23] E. McGuire, Atomic M-shell Coster-Kronig, Auger, and radiative rates, and fluorescence yields for Ca-Th, *Phys. Rev. A* 5 (3) (1972) 1043–1047.
- [24] S. Segui, S. Limandri, M. Torres Deluigi, C. Montanari, D. Mitnik, A. Carreras, G. Castellano, J. Trincavelli, $M\beta$ photon self-attenuation across the M_3 edge for elements with $70 \leq Z \leq 80$, in: XXXIII International Conference on Photonic, Electronic and Atomic Collisions, ICPEAC 23, 2023, p. 269.
- [25] J.A. Bearden, A.F. Burr, Reevaluation of X-Ray atomic energy levels, *Rev. Modern Phys.* 39 (1967) 125–142, <http://dx.doi.org/10.1103/RevModPhys.39.125>.
- [26] K. Sevier, Atomic electron binding energies, *At. Data Nucl. Data Tables* 24 (1979) 323, [http://dx.doi.org/10.1016/0092-640X\(79\)90012-3](http://dx.doi.org/10.1016/0092-640X(79)90012-3).